Supercritical Gel Drying: A Powerful Tool for Tailoring Symmetric Porous PVDF−HFP Membranes

S. Cardea,*,† A. Gugliuzza,‡ M. Sessa,† M. C. Aceto,‡,§ E. Drioli,‡,§ and E. Reverchon†

Department of Chemical and Food Engineering, University of Salerno, Via Ponte Don Melillo 1, 84084 Fisciano, Italy, Research Institute on Membrane Technology, ITM-CNR, c/o University of Calabria, Via Pietro Bucci 17C, 87036 Rende (CS), Italy, and Department of Chemical Engineering and Materials, University of Calabria, Via Pietro Bucci 17C, 87030 Rende, Italy

ABSTRACT In this work, poly(vinylidene fluoride) copolymer with hexafluoropropylene (PVDF−HFP) membrane-like aerogels have been generated for the first time. PVDF−HFP gels have been prepared from polymer−acetone solutions by adding various amounts of ethanol. A series of supercritical drying experiments have been performed at different pressures (from 100 to 200 bar) and temperatures (from 35 to 45 °C) and at various polymer concentrations (from 5 to 12 wt %). The effects of the process conditions on the membrane morphology have been evaluated, and structure−property relationships have been found. In all cases, the membranes exhibit interconnected structures with nanosized pores and high porosity, leading to reduced resistance to the gas mass transfer and high hydrophobic character of the surfaces. These membrane-like aerogels promise to form a new class of highly hydrophobic porous interfaces, potentially suitable to be used in membrane operations based, for example, on the contactor technology.

KEYWORDS: membranes • aerogels • supercritical CO_2, interfaces • contactors

INTRODUCTION

The copolymer of poly(vinylidene fluoride) with hexafluoropropylene (PVDF−HFP) is an acid-resistant, inert, and semicristalline material. Traditionally, PVDF membranes find large application in advanced fields of contactor technology (1), catalysis (2−4), biomedicine (5−8), as well as transductors (9) for the polymorphism that characterize this material. Because of these important technological applications, many works have been developed with the aim of producing porous PVDF−HFP structures (1, 10−20), emphasizing often the events controlling the phase-separation phenomena (1, 13, 19). However, porous PVDF membranes prepared according to traditional dry−wet processes rarely exhibit well-controlled morphology and chemistry, which are characteristics necessary to make them the ideal interfaces for membrane operations such as, for example, contactors (1). Non-well-defined pore size and pore distribution, coalescence phenomena, low surface, and overall porosity influence, in turn, the final performance of the membranes, producing interfaces not suitable for promoting the uniformity and high productivity of the process (21). In addition, the lack of hydrophobicity due to the use of hydrophilic pore formers affects significantly the waterproofness of the films, reducing the period of operational time. Recently, PVDF−HFP membranes have also been generated by a new technique in which supercritical carbon dioxide (SC-CO_2) replaces the liquid nonsolvent (i.e., SC-IPS process) (22−24). Compared to the dry−wet process, the SC-IPS process can give several advantages: SC-CO_2 substitutes the nonsolvent, reducing the potential pollution; the membrane is obtained without additional post-treatments because SC-CO_2 completely extracts the solvent; it is possible to modulate the membrane morphology, cells, and pore sizes simply by changing the operative conditions (22−34). The results obtained in the case of PVDF−HFP membranes confirmed the versatility of the process (through a change in the SC-CO_2 solvent power, either a leafy morphology or a cellular structure was obtained (22), but skinned surfaces were always obtained 22−24).

Another interesting process that could be a valid alternative for the preparation of porous membranes is the gel drying process (35−37). Unlike the phase-inversion process, the starting sample is a gel (not a solution) and the porous structure (i.e., aerogel) is formed during the gelation process; this process can assure a uniform and symmetric skinless nanostructured aerogel morphology, but some drawbacks can seriously affect gel formation. The surface tension of the solvent to be eliminated can cause the collapse of the gel polymeric structure (due to the cohesive forces between the liquid solvent and the polymeric nanosized network), leading to a partially nonporous structure, and long processing times are usually necessary. For these reasons, the removal of the solvent from the gel, without damaging the overall network of the polymer, represents an attractive strategy for the

* Corresponding author. Tel.: +39(0)89964232. Fax: +39(0)89964057. E-mail: scardea@unisa.it.
Received for review October 7, 2008 and accepted December 10, 2008
† University of Salerno.
‡ Research Institute on Membrane Technology, ITM-CNR, c/o University of Calabria.
§ Department of Chemical Engineering and Materials, University of Calabria.
DOI: 10.1021/am800101a

realization of well-patterned aerogels that could be useful as porous membranes.

In literature, some attempts to prepare membranes by means of the gel drying process have been reported by Cho and Lee (35). PVDF gels were prepared from PVDF/γ-butyrolactone solutions by using a hot-air-assisted drying process. Nonporous structures characterized by polymeric particles were obtained. Dasgupta et al. (36, 37) studied two different drying processes to obtain membranes. In the first work (36), the gels were obtained from PVDF/organic diester solutions that were then immersed in a cyclohexane bath for 12 h to replace the solvent into the gels. The process was repeated for 6−7 days. Then, the gels were dipped into methanol for 1 day and, finally, dried in a vacuum at 60 °C for 3 days, yielding partially porous structures. In a subsequent work, Dasgupta et al. (37) tried to avoid the collapse of the structure starting from a PVDF/camphor solution. In this way, they removed the solvent exploiting its tendency to easily sublimate under near-"freeze-drying" conditions. However, the drying time was longer. A new method to avoid the collapse of the structure and to obtain porous structures in a shorter time was presented by Daniel et al. (38); a SC-CO_2-assisted drying process was used for the formation of syndiotactic polystyrene aerogels finalized to the production of polymeric manufacts. The aerogel formation was obtained in a single step, preventing the structure of the gel from collapsing.

In the present work, a SC-CO_2-assisted drying process is proposed for the first time as a powerful nonconventional approach to fabricating porous PVDF−HFP membranes. The supercritical fluid has been used to dry the gel, resulting in stable aerogels having structures like that of skinless membranes with high overall porosity. This technique provides further multifaceted advantages with respect to the traditional phase-inversion techniques: uniform nanosized porous PVDF−HFP membranes can be generated in only one step without using hydrophilic pore formers; stable membrane networks can be achieved by removing simultaneously all solvents in an ecofriendly way; the solvent recovery can be performed by simply depressurizing the system; the methodology results in reduced costs and shorter time. Changes in the final membrane morphology and pore size, transport, and surface properties have been analyzed as a function of process parameters such as the polymer concentration, pressure, and temperature. The aerogels prepared according to this new approach exhibit a good performance when working as membranes. The supercritical-assisted drying approach promises, therefore, to become a strategic alternative to the traditional methods for the fabrication of a new class of porous PVDF−HFP membranes suitable for advanced chemical separations.

MATERIALS AND METHODS

Materials. PVDF−HFP (number average 199×10^3, weight average 353×10^3, polydispersity 1.8, density 1.78 g cm^{-3}) was kindly supplied by Solvay SA (Ixelles, Belgium); acetone (purity 99.5%, Sigma-Aldrich, St. Louis, MO) was used as the solvent and ethanol as the nonsolvent for formation of the gel (purity 99.8%, Sigma-Aldrich, St. Louis, MO); CO_2 (purity 99%) was purchased from Società Ossigeno Napoli (Napoli, Italy). Gases (CO_2, CH_4, and O_2) for permeation experiments were used as received (purity 98%, Pirossigeno Company, Cosenza, Italy). Ultrapure water was used for contact-angle measurements (filtered by the USF ELGA plant). A total of 12 measurements were done and averaged, and the plateau values were compared. All materials were processed as received.

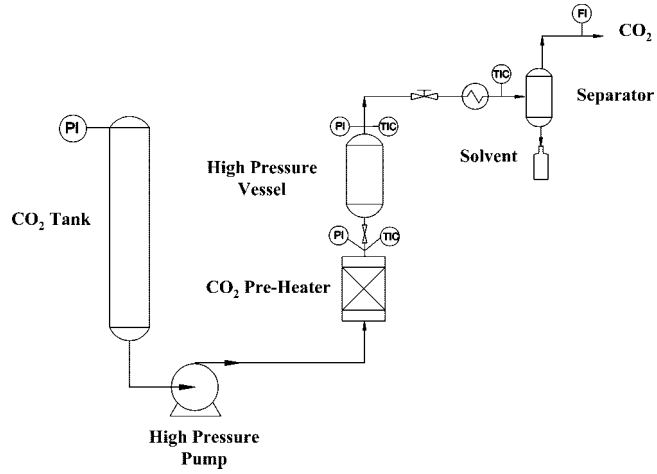

FIGURE 1. Experimental apparatus.

Table 1. Composition of the Gels Prepared

acronym	PVDF−HFP [wt %]	acetone [wt %]	ethanol [wt %]
A	5	60	35
B	7	60	33
C	10	60	30
D	12	60	28

Preparation of Aerogels Like Membranes. Gels of PVDF−HFP were prepared by dissolving the polymer in acetone under vigorous stirring at concentrations ranging from 5 to 12 wt %. Then, different amounts of ethanol were added to the homogeneous solution warmed at 50 °C (Table 1). Each polymer solution (i.e., dope) was placed in a formation cell (steel caps with a diameter of 2 cm). The formation cell was reposed in a freezer at −20 °C until a gel was formed (∼1 h). The drying process was performed in a laboratory apparatus equipped with a 316 stainless steel high-pressure vessel with an internal volume of 80 mL, in which SC-CO_2 contacts the polymer gel in a single pass (Figure 1). The gel was placed in the vessel, which was closed and filled from the bottom with SC-CO_2 up to the desired pressure using a high-pressure pump (Milton Roy Milroyal B). The time elapsed before SC-CO_2 contacted the gel was around 60 s. The apparatus operated in a continuous mode for 1 h, i.e., with a constant CO_2 flow rate of 1.5 kg h^{-1}. At the end, the vessel was slowly depressurized for 10 min and the aerogels were depleted from the support. The operative conditions of pressure and temperature were modified, ranging from 100 to 200 bar and from 35 to 45 °C, respectively.

Gelation Boundaries. A phase diagram of the PVDF−HFP/acetone/ethanol system was obtained by dropwise addition of the nonsolvent (ethanol) under continuous stirring at 25 °C (Figure 2). The gelation point was visually observed by means of the increased viscosity of the solution (13). The maximum concentration of polymer in the starting solution was 20 wt % in acetone. Further additions of polymer were limited either by the excessive viscosity of the solution, which produced inefficient stirring, or by a too strong inherent turbidity of the polymer dopes. The diagram in Figure 2 is thus an isotherm (at 25 °C) for the ternary system PVDF−HFP/acetone/ethanol. The gelation boundary "moves" inside the diagram through a

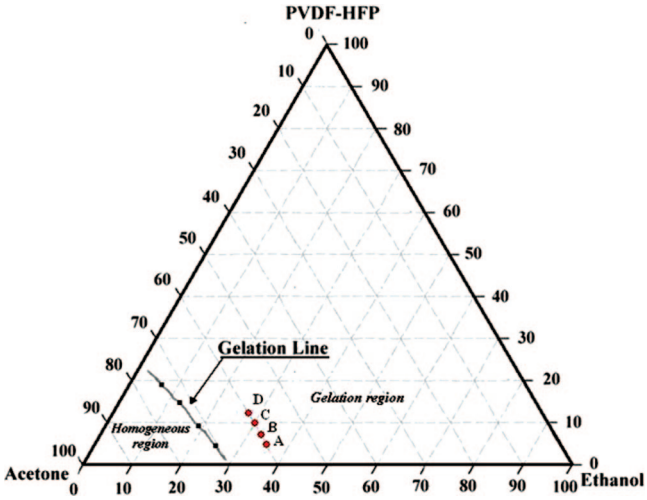

FIGURE 2. Phase diagram of the PVDF−HFP/acetone/ethanol system at 25 °C with a gelation line and with processed gel compositions (A, 5%/60%/35%; B, 7%/60%/33%; C, 10%/60%/30%; D, 12%/60%/28%).

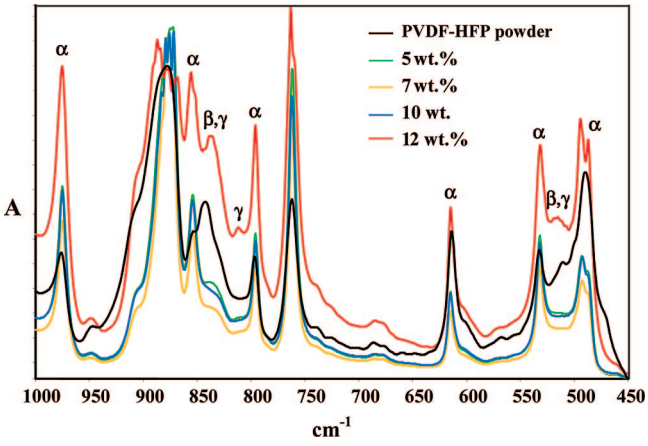

FIGURE 3. IR spectra collected on polymer powder and membrane-like aerogels at different polymer concentrations.

change in the temperature of the solution. In particular, upon warming of the solution (for example, up to 50 °C), the gelation boundary shifts toward the PVDF−HFP/ethanol axis and the homogeneous region largely increases. Upon cooling of the solution (for example, at −20 °C), the gelation boundary shifts toward the acetone apex, leading to a smaller homogeneous region.

Aerogel Crystallinity. Changes in the aerogel crystallinity were detected for all samples by thermal analysis using Diamond Pyris differential scanning calorimetry (DSC; Perkin Elmer, Waltham, MA). To obtain an identical thermal history, each sample was heated from 50 to 200 °C at 15 °C min^{-1}, cooled down to 50 °C, and heated again up to 200 °C. The weighed amount of sample for each experiment was approximately 8.0 mg. The heat flow was normalized by the sample weights. All transitions were compared with those of the polymer powder. IR spectra were also collected in transmission mode at a resolution of 4 cm^{-1} from each sample using a Spectrum One System (Perkin Elmer, Waltham, MA) and compared with that of the untreated polymer powder.

Morphology and Topography Analyses. PVDF−HFP aerogels were cryofractured by a microtome (Bio-optica SpA, Milano, Italy; model Microm HM 550 OMVP). The samples were sputter coated with gold and observed by a scanning electron microscope (SEM; model LEO 420, Assing, Italy) to study the film structure. The membrane topography was estimated using

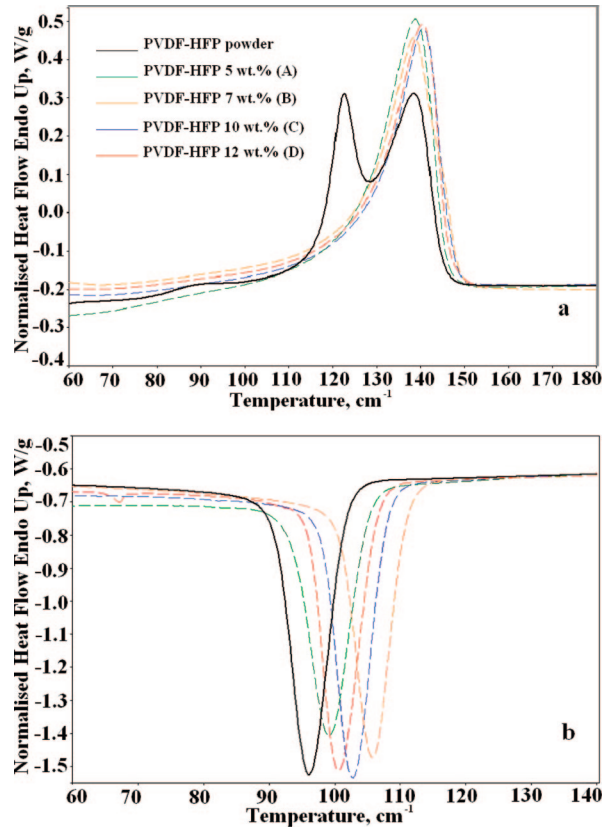

FIGURE 4. DSC analysis performed on polymer powder and membranes: (a) first heating run; (b) cooling run.

atomic force microscopy (AFM; Nanoscope III Digital Instruments, VEECO Metrology Group). AFM was operated in tapping mode by a tip attached to the end of an oscillating cantilever across 10 × 10 μm^2 of sample surface at a rate of 1.0 Hz. The pore size, pore distribution, and surface porosity were estimated from AFM images. The pore size was a log-normal distribution for all membranes; the cumulative distribution function versus the ascending pore size was a straight line on log-normal probability paper. The mean pore size was calculated from the log-normal plot, and the pore distribution was expressed by the probability density function [df(dp)/dp, μm^{-1}] according to ref19.

The overall porosity (ϵ), expressed as the "void volume fraction" inside the membrane, was calculated from the apparent density of the membrane (ρ_m) and the density of the PVDF−HFP powder (ρ_p = 1.78 g cm^{-3}). The apparent membrane density was determined by measuring the volume and the weight of the film. This operation was performed on 10 samples for each experimental condition with a standard deviation of 0.02.

To confirm the estimated porosity values and evaluate the interconnectivity degree into the bulk of the films, specimens of various samples were filled by a liquid characterized by a low surface tension (Fluorinert FC40, 3M Novec) and the void volume fraction was calculated from the weight and density of the solvent adsorbed inside the open pores.

Evaluation of Gas Transport through the Membranes. Permeation experiments to some gases (CO_2, CH_4, and O_2) were also performed at 1 bar and 25 °C according to the fixed volume−pressure increase mode. Four specimens of membrane samples with an effective area of 2.14 cm^2 were tested. The experimental error was ≤10%.

Contact-Angle Measurements. The wetting degree was estimated by dynamic contact-angle experiments. The technique used consisted of the sessile drop method by a CAM 200

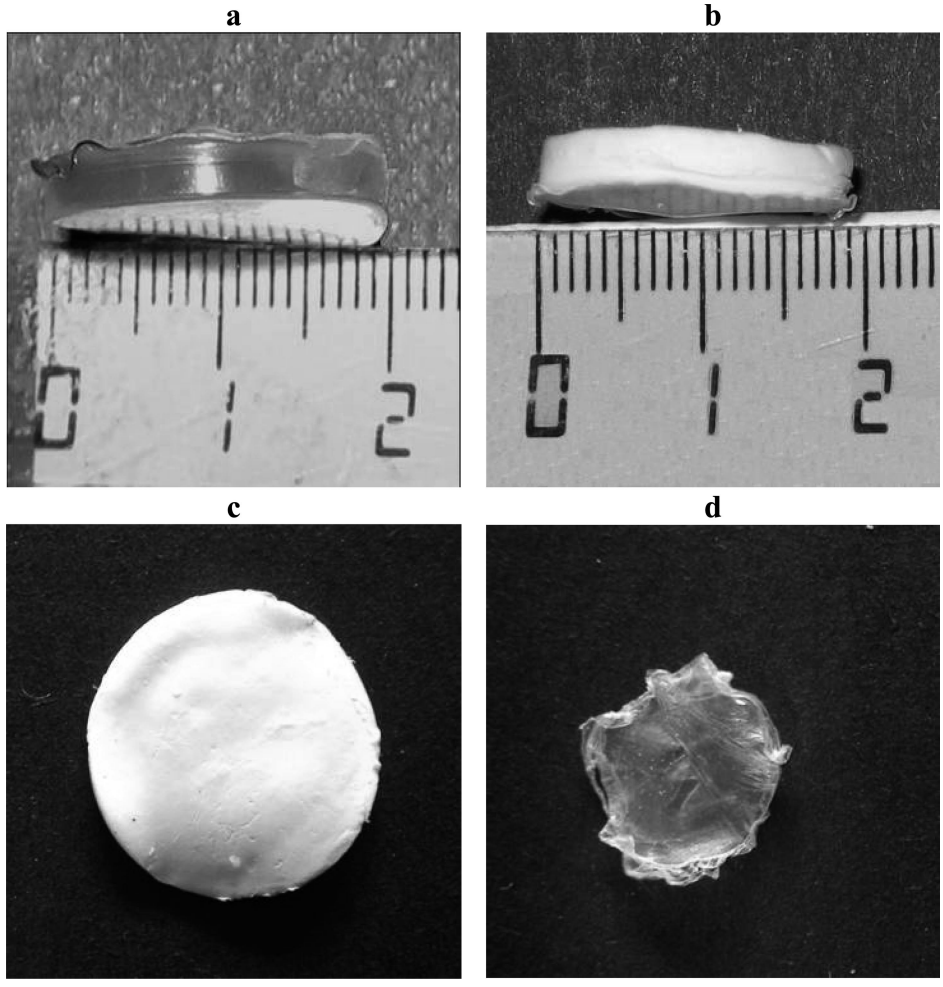

FIGURE 5. (a) Gel obtained with 10 wt % of PVDF−HFP. (b and c) Membrane-like aerogel with 10 wt % of PVDF−HFP obtained by supercritical drying. (d) PVDF−HFP nonporous polymeric film obtained by air drying.

contact-angle meter (KSV Instruments Ltd., Helsinki, Finland). The water droplets were deposited on the membrane surface using a microsyringe with an automatic dispenser; the images were captured by a digital camera. An average of 15−20 readings were carried out for each specimen, and the mean value was then calculated.

RESULTS AND DISCUSSION

Gelation Region for the PVDF−HFP/Acetone/Ethanol System. The gelation boundary of PVDF−HFP in acetone/ethanol solutions was determined by identifying the equilibrium gelation points, which are the compositions at which the homogeneous solutions form solid structures embedded in the liquid system (gels) at 25 °C. Experimental determination of the gelation region was limited to a maximum polymer concentration of 20 wt % to avoid inefficient stirring because of a very high solution viscosity (Figure 2). As is possible to observe in Figure 2, the gelation line of the solution is very close to the solvent apex, confirming the tendency of the copolymer PVDF−HFP to produce these kinds of structures as already observed in the literature (11, 22, 39−40); indeed, the ternary phase diagrams show large gelation regions for these kinds of polymers, where precipitation by solid−liquid demixing predominates on that liquid−liquid, resulting in membranes with different morphologies (22, 41).

Membrane-like Aerogels. ***Gelation Process.*** The gel drying process allows one to obtain polymeric aerogels, i.e., to eliminate the liquid solvent, avoiding the collapse of the gel solid structure; one of the possible aerogel structures is formed by a nanostructured network of polymeric fibers (38).

Using SC-CO_2 drying, various PVDF−HFP gels were prepared by changing the polymer concentration from 5 to 12 wt % and keeping the concentration of acetone constant at 60 wt % (Table 1). The concentration of the ethanol was varied proportionally to the polymer concentration. At 50 °C, the polymer dope compositions lie in the homogeneous region; the subsequent freezing of the solution at temperatures down to −20 °C leads the mixtures into the gelification region that is more extended at lower temperatures, as discussed in the paragraph on "gelation boundaries". The mixtures remain in the gelation region when raised again to the ambient temperature (25 °C) (Figure 2).

The PVDF tendency to form gel is mainly due to the semicrystalline character of the polymer. The solutions move quickly inside the crystallization region when aided by a soft nonsolvent like ethanol. This enters the polymer dopes into the crystallization region where a solid−liquid demixing occurs. Gels with high crystalline character are then formed.

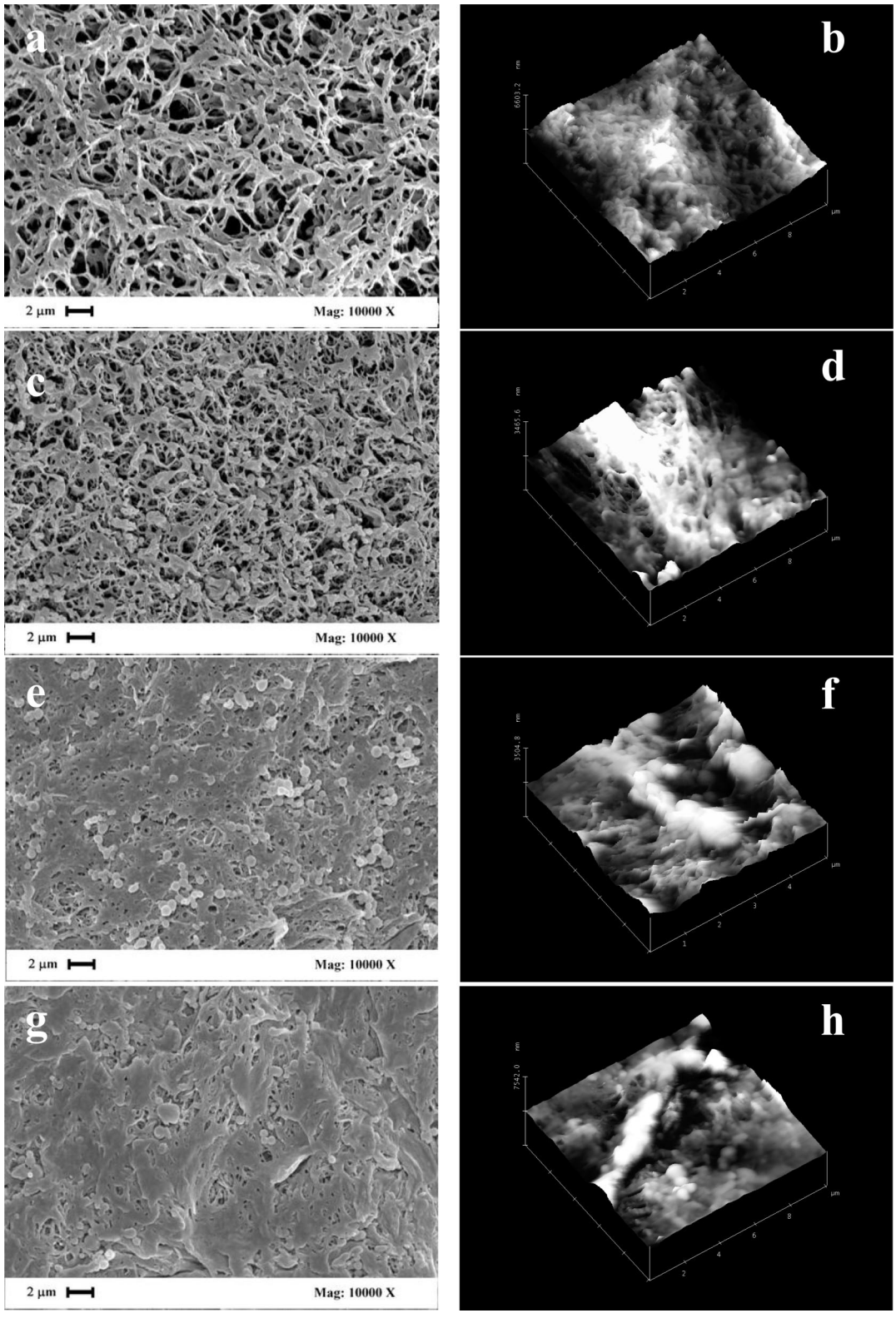

FIGURE 6. SEM (magnification: 10 000×) and AFM (area scan size: 10 × 10 μm^2) images of the membrane surfaces obtained at 200 bar and 35 °C: (a and b) 5 wt %, (c and d) 7 wt %, (e and f) 10 wt %, and (g and h) 12 wt % of PVDF−HFP.

With this regard, IR spectroscopy and thermal analysis provided useful information about the changes occurring in the membrane crystallinity as the polymer and ethanol concentrations were varied in the mixture (Figures 3 and 4).

The dissolution of the polymer in acetone reduces drastically the crystalline domains in favor of the most stable and nonpolar α phase. This is confirmed by both the disappearance of the melting peak at 112 °C and the reduced enthalpy of fusion of the aerogels. Despite the highest thermodynamic stability and predominance of the α phase, a significant presence of β and γ forms is observed for the aerogels formed from gels A and D, as indicated by the increased

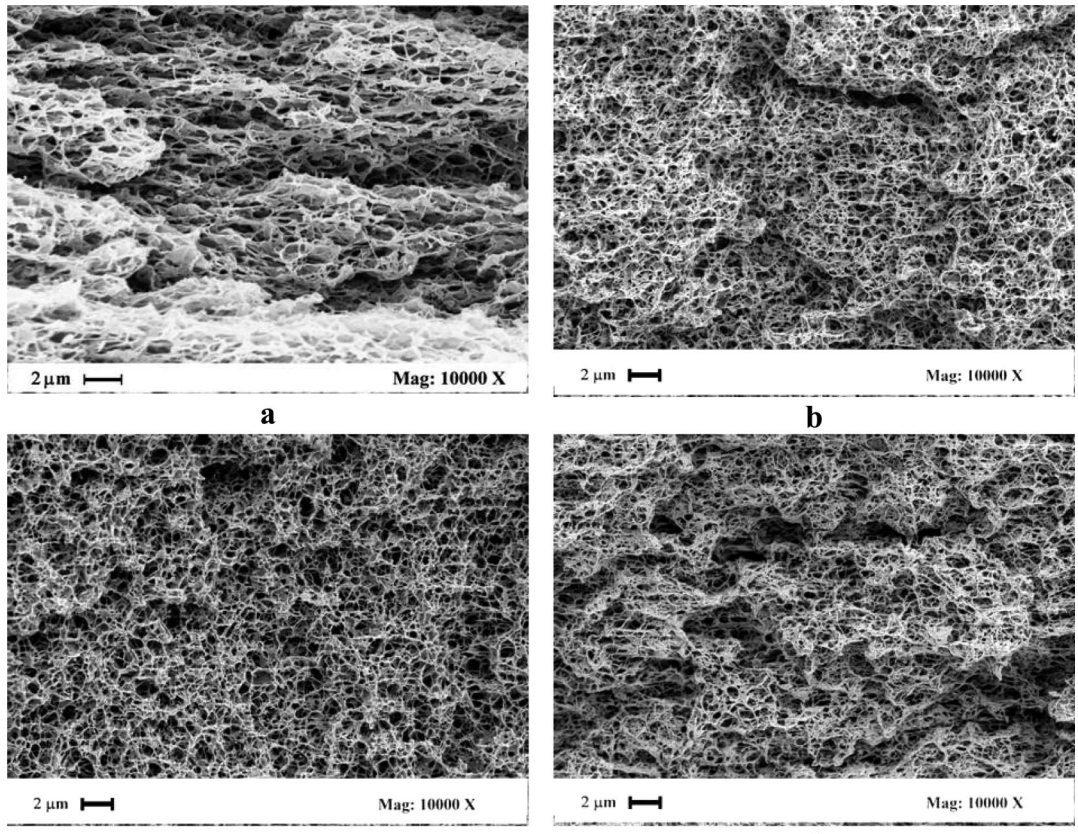

FIGURE 7. SEM images of the cross sections of membrane-like aerogels prepared at 200 bar and 35 °C: (a) 5 wt %, (b) 7 wt % (c) 10 wt %, and (d) 12 wt % of PVDF−HFP.

vibrational modes typically ascribed to the stretching bands of the β and γ forms (Figure 3). Further confirmation of the higher crystalline content is given by a somewhat larger enthalpy of fusion (48 J g^{-1}) than that estimated for the other aerogels (44 J g^{-1}) during the first heating run (Figure 4) as well as by the changes in the supercooling of the crystallization occurring during the cooling run. Indeed, different positions of the crystallization peaks are present. Both aerogels A and D exhibit a crystallization temperature close to 100 °C, slightly higher than that of the polymer powder (96 °C). In contrast, higher crystallization temperatures were estimated for the other two aerogels (B and C). This suggests that the crystalline nucleus compositions of aerogels A and D are comparable. At higher polymer content, the high supersaturation degree of the solution promotes the nucleation and growth of various crystalline forms, resulting in a high polymorphic degree of the aerogel. When the polymer concentration is reduced, a proportional amount of nonsolvent is added to the solution, making favorable environments for the nucleation of polymorphic species.

Effect of Supercritical Fluid Processing. The obtainment of supercritical conditions plays a crucial role in the fabrication process of stable membrane-like aerogels. As described above, SC-CO_2 rapidly eliminates all of the solvents, transforming the gel in aerogel and preserving the nanosized polymeric structure. Indeed, CO_2 at supercritical conditions can be considered as a zero-surface-tension compound; when it diffuses inside the PVDF−HFP gels, an acetone/ethanol/SC-CO_2 mixture is formed. Also, this mixture presents a surface tension near zero, and it can be removed from the nanosized polymeric network without mechanical stress for the structure because no cohesive forces are present.

Parts a−c of Figure 5 show an example of a PVDF−HFP-based gel obtained starting from a mixture at 10% in polymer, 60% in acetone, and 30% in ethanol. The aerogel formed by the SC-CO_2-assisted process (Figure 5b,c) preserves both the dimension and shape exhibited by the gel before the drying treatment, respectively (Figure 5a). On the contrary, the same gel, dried in hot air, exhibits a completely collapsed dense structure (Figure 5d). The SC-CO_2-assisted drying process is, therefore, meant to overcome the drawback related to the collapse of the polymer network. Indeed, the fast removal of the solvent avoids the weakening of the matrix and then the destruction of the aerogel. In addition, the high SC-CO_2 solvent power together with the absence of surface tension at supercritical conditions avoids the presence of traces of solvent inside the aerogels at the end of the process. The result is a well-dried aerogel having the structural stability necessary to work as a membrane.

Effect of the Polymer Concentration. All polymer dopes that we used are inside the gelation boundary at 25 °C, with different solvent/nonsolvent ratios. Shock freezing quickly enters the dopes in the gelation area, leading to denser structures at higher degrees of supersaturation (i.e., at higher polymer concentrations) as shown in Figure 6. All

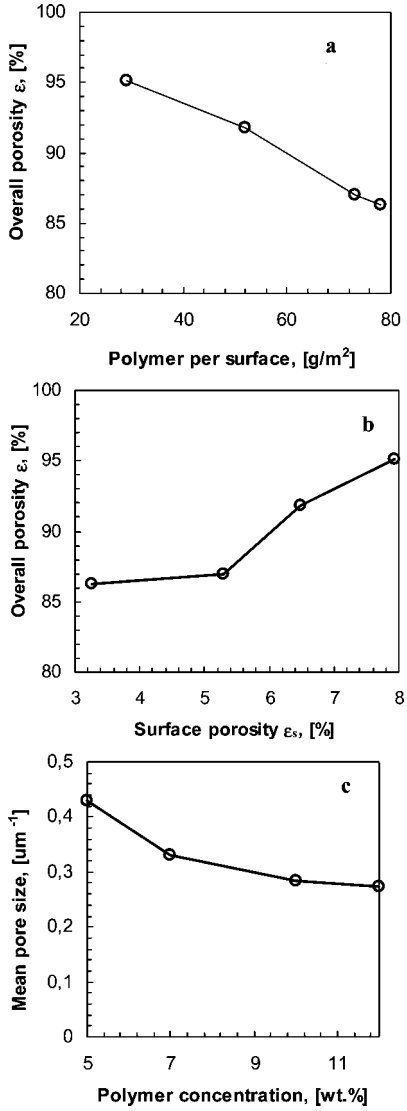

FIGURE 8. Relationships between the overall void volume fraction and (a) the polymer amount per membrane surface, (b) the surface porosity estimated by AFM analysis, and (c) the geometric mean pore size as a function of the polymer concentration.

membranes exhibit fibrous structures, but nodulelike morphology occurs significantly on membranes prepared from higher polymer concentration mixtures. SEM and AFM images show more compacted and skinned structures because the initial polymer contents in the mixture are 10 and 12 wt % (Figure 6c,d); however, the particulate-like morphology predominates on the top layer of the membrane surfaces, suggesting a dependence from the local polymer concentration and the tendency of the polymer to minimize the surface energy, forming solid spheres. Small amounts of acetone tend to evaporate before contacting the supercritical fluid. This could produce a further increase in the polymer concentration at the gel/air interface, resulting in an increased degree of supersaturation and leaving nodule aggregates.

In contrast, open and reduced spherulitic structures characterize the membranes derived from solutions at lower polymer concentration (5 and 7 wt %; Figure 6a,b). This fact suggests a slower occurrence of crystallization-induced gelation, resulting in a bigger critical nucleus size and then in larger porosity. As a result, aerogels like skinless membranes are formed.

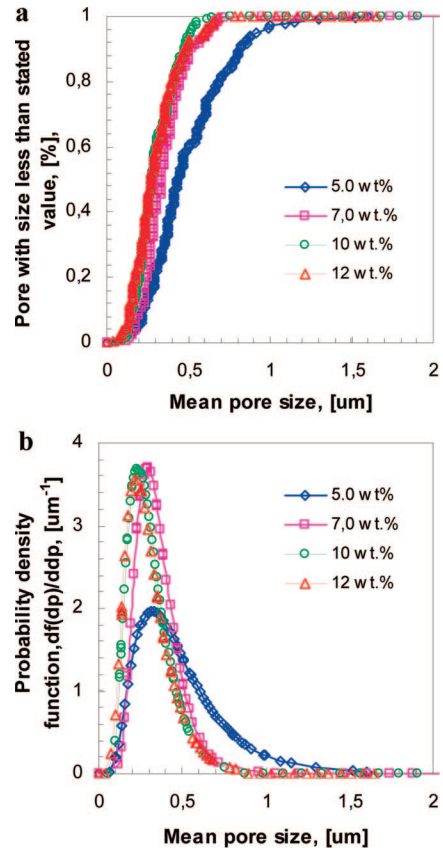

FIGURE 9. Evaluation of the changes in the geometric mean pore size measured from AFM images: (a) cumulative distribution of the pore sizes; (b) probability density function curves built up from the pore sizes measured from AFM.

All membranes obtained from PVDF gels by the SC-CO_2-assisted drying process exhibit uniform and symmetric structure across the overall section of the layers, as well illustrated by SEM images (Figure 7); indeed, SEM analysis was performed on different zones of each sample to testify to the uniformity and symmetry of the structures obtained. This result was also confirmed by other analyses performed on the membranes (DSC, AFM, and IR): each analysis was performed several times on different zones of each membrane, resulting in comparable results.

When the cross sections of all films are compared, an increase in the overall porosity can be appreciated with decreasing polymer concentration. An inverse proportionality between the void volume fraction (ϵ, %) and the amount of polymer per unit of surface (G, g m^{-2}) was, therefore, estimated (Figure 8a). On the contrary, a linear increase between the overall and surface porosities was observed (Figure 8b). This suggests a uniform increase in the formation of liquid micelles during the nucleation stage of gelation, leaving a slightly larger and uniformly distributed pore size as the polymer concentration decreased (Figure 8c). Changes in the porosity are, therefore, the result of a gradual tendency of the pore size to increase with decreasing polymer concentration, as was well quantified by AFM measurements

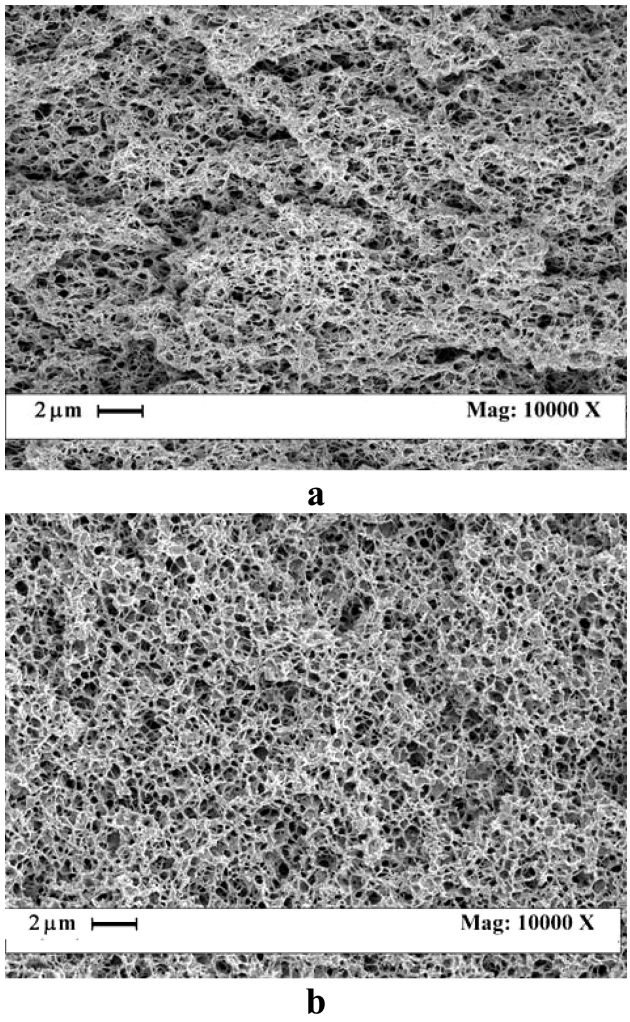

FIGURE 10. Effect of the pressure on the final morphology and the cell size of membrane-like aerogels prepared from gels with 10 wt % of PVDF−HFP at 35 °C and two different operating pressures: (a) 200 bar; (b) 100 bar.

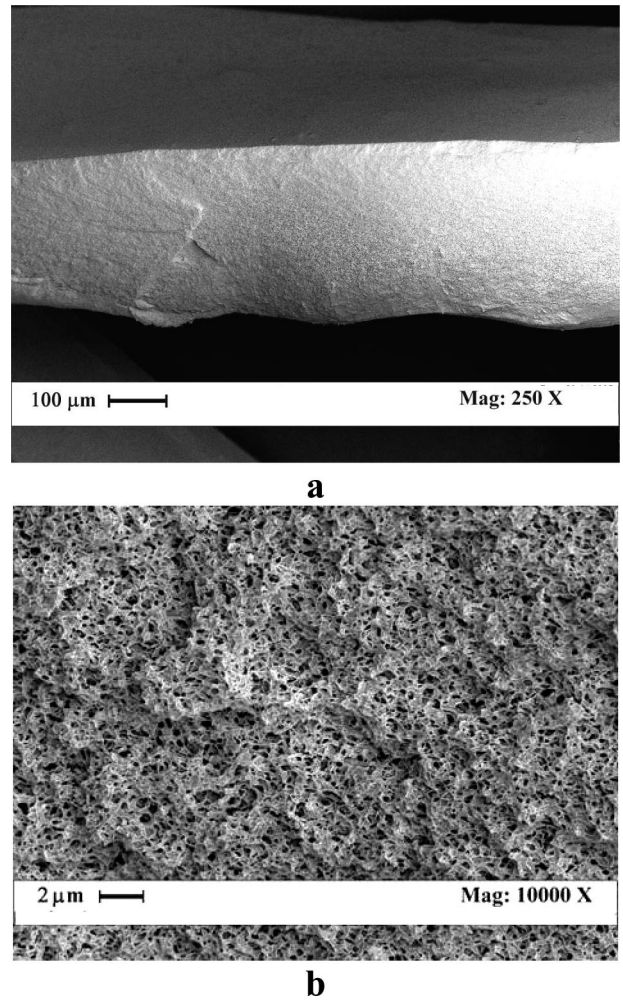

FIGURE 11. SEM images of PVDF−HFP membrane-like aerogels obtained at 200 bar and 45 °C: (a) whole section; (b) internal structure.

(Figures 8c and 9). All plots of the median ranks versus the increasing pore sizes on the log-normal probability paper were linear with correlation coefficients $\geq 0.90 r^2$ (Figure 9a). Unimodal pore distributions were estimated for all membranes, even if a broadening of the distribution was obtained for membranes prepared at 5 wt % of polymer (Figure 9b). This fact could be ascribed to coalescence phenomena occurring in the polymer-lean region during gel formation.

The obtainment of values of overall porosity up to 95% with the complete suppression of macrovoids is an important result with respect to traditional PVDF−HFP membranes, where fingerlike structures are often combined with dense skin layers. On the other hand, a uniform distribution of the void volume fraction through the overall film is a crucial factor for the productivity of most of the membrane operations, but it gains particular importance if the membrane is used to equip, for example, contactor devices.

Effect of the Pressure and Temperature. Experiments were performed at different pressures, keeping the other process parameters constant (35 °C and 10 wt % of PVDF−HFP). A decrease in the pressure from 200 to 100 bar does not affect the overall porosity of the membranes, which remains constant (i.e., approximately 88%; Figure 10). This result can be explained considering that a pressure variation only changes the solvent power of SC-CO_2, which tends to increase with the pressure. Operating in this way, it is possible to dry the gel in a shorter time without influencing the membrane structure. In particular, the drying time decreased down to 30 min as the pressure increased from 100 to 200 bar. This result confirms that the aerogel structure is formed during the gelation process and not during the drying process. On the contrary, an increase in the temperature from 35 to 45 °C reduces dramatically the membrane porosity from 90% to 40%, resulting in a strong densification of the polymeric matrixes across the overall section (Figure 11). Specifically, the gel thickness decreases sensibly from 2 to 0.4 mm for membranes prepared from polymer dopes at 10 wt %, 45 °C, and 200 bar (Figures 10a and 11b), resulting in compact structures.

This result could be due to the volatility of the liquid solvents, which is responsible for an increase in the polymer-rich phases during the membrane formation; because the boiling point of acetone is 56.5 °C, a nonnegligible vaporization at a temperature of 45 °C is expected. This fact produces a decrease in the solvent/nonsolvent ratio, result-

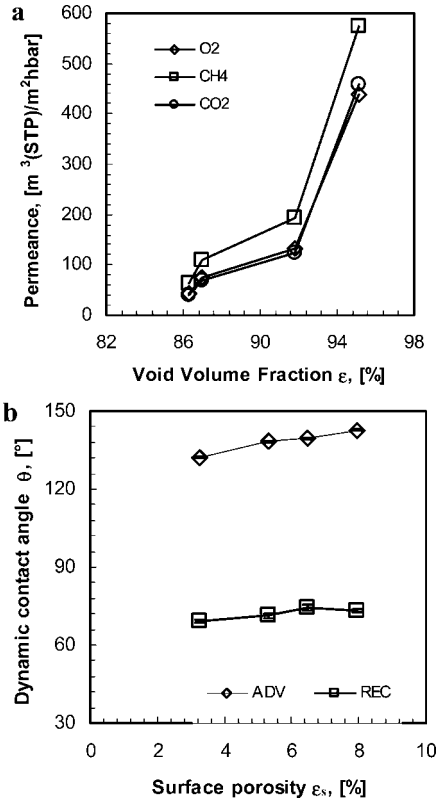

FIGURE 12. Transport property relationships assessed for PVDF–HFP membranes prepared by the SC-CO_2-assisted drying process: (a) correlation between the overall void volume fraction and rising gas mass transfer; (b) estimation of the wetting degree on the surface of all PVDF–HFP membrane-like aerogels.

ing in a reduction of the liquid micelle size and then in a major densification of the final structure.

Structure–Property Relationships. PVDF membranes achieved by the SC-CO_2-assisted drying process were tested to establish their suitability to work as nonselective interfaces for advanced applications such as contactor operations. One of the most important requirements of the contactor technology is the high mass transfer through the membrane. The target of high productivity can be achieved if a high overall porosity characterizes the membranes, resulting in a reduced resistance to mass transport.

Indeed, an increase in the overall porosity has been estimated with decreasing polymer concentration (Figure 8a) and rising surface porosity (Figure 8b) for all membrane-like aerogels. This characteristic produces a reduced resistance to the mass transfer into the bulk of the films and, therefore, high gas permeations (Figure 12a). When the permeation is compared to the various gases, the membranes exhibited a somewhat higher permeation to methane to be ascribed to the lowest molecular weight of this gas. Despite the fact that a convective flux can characterize the gas transfer through these membranes, a small Knudsen component in the mass-transfer mechanism cannot be excluded. Changes in the intrinsic structural parameters of the membrane-like aerogels also influence positively the final surface properties of the films in terms of controlled mutual liquid–membrane interactions. Indeed, another important achievement for processing hydrophobic membranes in contactor devices is, for example, the inhibition of spreading phenomena. Liquid water must be prevented from penetrating inside the membrane pores to keep the interface of the two media constant at the mouth of each single channel of the films. Thus, a high hydrophobic character of the surface has to be assured. Dynamic contact-angle experiments performed on the surface of the various membrane-like aerogels produced in this work confirmed the high hydrophobic character of the membranes (Figure 12b). As the polymer concentration decreased, an increase of the contact-angle values up to 143 ± 3° was observed, yielding useful information about the waterproofness of the membrane surfaces. A hysteresis of 66 ± 5° was calculated between the advancing and receding angles, because of surface roughness effects, responsible for the capture of hydrophobic air inside the membrane pores and, consequently, for the enhanced water repellence with increasing pore size (1). These aerogels are, therefore, suggested to form an interesting class of new membranes having the necessary structure–property characteristics for equipping contactor devices.

CONCLUSIONS

The SC-CO_2-assisted gel drying process is a promising approach for the fabrication of aerogels having characteristics useful for membranes equipping contactor devices. This technique offers the powerful advantage of producing stable symmetric membranes with nanosized pores, high porosity, and porous surface, avoiding the collapse of the structure due to the absence of surface tension of SC-CO_2. The polymer concentration is a crucial controlling parameter for changing the structural aspects of the films. The membrane-like aerogels exhibited, in turn, modulated pore size and porosity. These morphological achievements are responsible for the enhanced transport and surface properties of the membranes. In addition, these membrane-like aerogels exhibit polymorphic character, the crystalline composition of which could be usefully changed as a function of the solvent/nonsolvent ratio used. Finally, the manufacturing approach appears less expensive and ecosustainable with respect to traditional manufacturing approaches.

REFERENCES AND NOTES

(1) Gugliuzza, A.; Drioli, E. *J. Membr. Sci.* **2007**, *300*, 51>62.
(2) Buonomenna, M. G.; Drioli, E.; Nugent, W.; Prins, L.; Scrimin, P.; Licini, G. *Tetrahedron Lett.* **2004**, *45*, 7515–7518.
(3) Bottino, A.; Capannelli, G.; Comite, A. *Desalination* **2002**, *146*, 35–40.
(4) Bottino, A.; Capannelli, G.; Comite, A.; Di Felice, R. *Desalination* **2002**, *144*, 411–416.
(5) Guenard, V.; Valentini, R. F.; Aebischer, P. *Biomaterials* **1991**, *12*, 259–263.
(6) Chen, H.; Soldani, G.; Galletti, P. M.; Goddard, M. *ASAIO J.* **1992**, *38*, 201–206.
(7) Grandien, J. D. U.S. Patent 4,203,847, 1980.
(8) Karakulski, K.; Morawski, W. A.; Grzechulska, J. *Sep. Purif. Technol.* **1998**, *14*, 163–173.
(9) Gregorio, R.; Cestari, M. *J. Polym. Sci., Part B: Polym. Phys.* **1994**, *32*, 859–870.
(10) Lin, D. J.; Chang, H. H.; Chen, T. C.; Lee, Y. C.; Cheng, L. P. *Eur. Polym. J.* **2006**, *42*, 1581–1594.
(11) Young, T. H.; Cheng, L. P.; Lin, D. J.; Fane, L.; Chuang, W. Y. *Polymer* **1999**, *40*, 5315–5323.
(12) Deshmukh, S. P.; Li, K. *J. Membr. Sci.* **1998**, *150*, 75–85.

(13) Cheng, L. P.; Lin, D. J.; Shih, C. H.; Dwan, A. H.; Gryte, C. C. *J. Polym. Sci., Part B: Polym. Phys.* **1999**, *37*, 2079–2092.
(14) Wang, D.; Li, K.; Teo, W. K. *J. Membr. Sci.* **2000**, *178*, 13–23.
(15) Wang, M. D.; Li, K.; Teo, W. K. *J. Membr. Sci.* **1999**, *163*, 211–220.
(16) Yan, L.; Wang, K.; Ye, L. *J. Mater. Sci. Lett.* **2003**, *22*, 1713–1717.
(17) Tomaszewska, M. *Desalination* **1996**, *104*, 1–11.
(18) Feng, C.; Shi, B.; Li, G.; Wu, Y. *J. Membr. Sci.* **2004**, *237*, 15–24.
(19) Khayet, M.; Feng, C. Y.; Khulbe, K. C.; Matsuura, T. *Polymer* **2002**, *43*, 3879–3890.
(20) Chen, N.; Hong, L. *Polymer* **2002**, *43*, 1429–1436.
(21) Gugliuzza, A.; Aceto, M. C.; Macedonio, F.; Drioli, E. *J. Phys. Chem. B* **2008**, *34*, 10483–10496.
(22) Reverchon, E.; Cardea, S. *Ind. Eng. Chem. Res.* **2006**, *45*, 8939–8945.
(23) Cao, J. H.; Zhu, B. K.; Ji, G. L.; Xu, Y. Y. *J. Membr. Sci.* **2005**, *266*, 102–109.
(24) Huang, S.; Wu, G.; Chen, S. *J. Membr. Sci.* **2007**, *293*, 100–110.
(25) Reverchon, E.; Cardea, S. *J. Membr. Sci.* **2004**, *240*, 187–195.
(26) Cardea, S.; Gugliuzza, A.; Schiavo Rappo, E.; Aceto, M.; Drioli, E.; Reverchon, E. *Desalination* **2006**, *200*, 58–60.
(27) Xu, Q.; Pang, M.; Peng, Q.; Li, J.; Jiang, Y. *J. Appl. Polym. Sci.* **2004**, *94*, 2158–2163.
(28) Xu, Q.; Pang, M.; Peng, Q.; Li, J.; Jiang, Y.; Wang, H.; Zhu, M. *J. Appl. Polym. Sci.* **2005**, *98*, 831–837.
(29) Reverchon, E.; Schiavo Rappo, E.; Cardea, S. *Polym. Eng. Sci.* **2006**, *46*, 188–197.
(30) Matsuyama, H.; Yamamoto, A.; Yano, H.; Maki, T.; Teramoto, M.; Mishima, K.; Matsuyama, K. *J. Membr. Sci.* **2001**, *194*, 157–163.
(31) Reverchon, E.; Cardea, S. *J. Supercrit. Fluids* **2005**, *35*, 140–146.
(32) Temtem, M.; Casimiro, T.; Aguiar-Ricardo, A. *J. Membr. Sci.* **2006**, *283*, 244–252.
(33) Temtem, M.; Casimiro, T.; Aguiar-Ricardo, A.; Mano, F. J. *J. Supercrit. Fluids* **2008**, *43*, 542–548.
(34) Reverchon, E.; Cardea, S.; Rapuano, C. *J. Appl. Polym. Sci.* **2007**, *104*, 3151–3160.
(35) Cho, J. W.; Lee, G. W. *J. Polym. Sci., Part B: Polym. Phys.* **1996**, *34*, 1605–1611.
(36) Dasgupta, D.; Manna, S.; Malik, S.; Rochas, C.; Guenet, J. M.; Nandi, A. K. *Macromol. Symp.* **2005**, *222*, 175–180.
(37) Dasgupta, D.; Nandi, A. K. *Macromolecules* **2005**, *38*, 6504–6512.
(38) Daniel, C.; Alfano, D.; Venditto, V.; Cardea, S.; Reverchon, E.; Larobina, D.; Mensitieri, G.; Guerra, G. *Adv. Mater.* **2005**, *17*, 1515–1518.
(39) Lin, D. J.; Chang, C. L.; Huang, F. M.; Cheng, L. P. *Polymer* **2003**, *44*, 413–422.
(40) Stephan, A. M.; Renganathan, N. G.; Gopukumar, S.; Teeters, D. *Mater. Chem. Phys.* **2004**, *85*, 6–11.
(41) Van de Witte, P.; Dijkstra, P. J.; Van den Berg, J. W. A.; Feijen, J. *J. Membr. Sci.* **1996**, *117*, 1–31.

AM800101A